Resonant unidirectional and elastic scattering of surface plasmon polaritons by high refractive index dielectric nanoparticles

Andrey B. Evlyukhin[1,2] and Sergey I. Bozhevolnyi[2]
[1]*Laser Zentrum Hannover e.V., Hollerithallee 8, D-30419 Hannover, Germany*
[2]*Centre for Nano Optics, University of Southern Denmark, Campusvej 55, DK-5230 Odense M, Denmark*
(Received 3 September 2015; revised manuscript received 23 November 2015; published 14 December 2015)

We consider scattering of surface plasmon polaritons (SPPs) and light by individual high refractive index dielectric nanoparticles (NPs) located on a metal (gold) substrate and supporting electric and magnetic dipole resonances in the visible spectral range. Numerical calculations are carried out by making use of the discrete dipole approximation including the multipole decomposition procedure. Extinction and scattering cross-section spectra of spheroid silicon NPs in visible and near infrared are presented and discussed. The roles of the in-plane and out-of-plane components of electric and magnetic dipoles in the scattering processes are clarified and demonstrated. It is revealed that, owing to the NP interaction with electromagnetic fields reflected from the substrate (that leads to bianisotropy), the in-plane electric and magnetic dipoles can resonantly be excited at the same wavelength. Due to this effect, the resonant unidirectional (forward) and elastic (in-plane) scattering of SPPs by oblate spheroid NPs can be realized within a narrow spectral range. In the case of normal light incidence, the bianisotropy effect can provide significant suppression of the SPP excitation because of the destructive interference between the SPP waves generated by induced electric and magnetic dipole moments. The results obtained open new possibilities for the development of SPP-based photonic components and metasurfaces, whose operation involves resonant excitations of dielectric NPs.

DOI: 10.1103/PhysRevB.92.245419 PACS number(s): 78.68.+m, 71.36.+c, 02.70.−c, 03.65.Nk

I. INTRODUCTION

Surface optical electromagnetic waves can be excited at the interface between a dielectric and a metal and are called surface plasmon polaritons (SPPs). One of the most attractive properties of SPPs is the possibility to concentrate and channel electromagnetic radiation using subwavelength structures [1–3]. Experimental studies demonstrated that ensembles of metal nanoparticles (NPs) arranged on metal surfaces can be used to realize efficient micro-optical elements for two-dimensional (2D) manipulation of SPP waves, such as mirrors, beam splitters, and interferometers [4–9]. Furthermore, periodic arrays of metal NPs have been shown to exhibit band-gap properties for SPPs [10]. If such an SPP band-gap structure has narrow channels free from NPs, then SPP waves can be confined to and guided along these channels [10].

From the theoretical point of view, the SPP scattering properties of individual metal NPs and NP ensembles mentioned above can efficiently be treated in the point-dipole approximation [11,12], with each NP being considered as an electric dipolar scatterer and the NP dipole moments being self-consistently determined by solving the couple-dipole equations [8,13]. It has been shown that electric dipolar NPs scatter SPP waves mainly isotropically, with only small modulation in the forward and backward directions with respect to the incident SPP propagation [12]. With increasing of NP sizes, higher multipole modes of NPs can be excited influencing and changing the SPP scattering diagrams [14], a feature that could be used for functional optimization of SPP-based components. It should, however, be borne in mind that metal NPs efficiently absorb the electromagnetic radiation at optical frequencies due to large Ohmic losses. This feature together with the (inelastic or out-of-plane) scattering SPP into light, propagating away from the metal surface [1,15], can significantly restrict the application potential of metal NP structures in 2D SPP optics.

It is possible to overcome this principal drawback of metal NPs and nanostructures by employing an alternative approach based on high refractive index dielectric or semiconductor NPs. Due to Mie resonances, the dielectric NPs can strongly interact with both electric and magnetic field components of optical waves [16]. Recently it has been shown both theoretically [17,18] and experimentally [19,20] that crystalline silicon NPs exhibit pronounced optical Mie resonances associated with the excitation of magnetic and electric dipole (MD and ED) modes in these NPs. Depending on NP sizes, the resonances can be realized within the visible or near-infrared spectral ranges, where the silicon dielectric permittivity has a very small imaginary part and the silicon NPs can be considered as high refractive index dielectric NPs. Because silicon NPs support resonant excitation of MD and ED modes, there appears a possibility to realize a strong unidirectional (forward) light scattering by satisfying the so-called Kerker condition [17,21,22]. Importantly, the spectral separation between the ED and MD resonances can be controlled by NP shapes and irradiation conditions [23], which gives a possibility to realize the resonant Kerker effect and to create novel metamaterials [24–26]. Resonant optical properties of high refractive dielectric NPs have been suggested for realization of new types of optical nanoantennas [27–29] and ultrahigh efficiency photovoltaic cells [30,31]. However, resonant interaction of high refractive index dielectric NPs with SPPs have not hitherto been considered.

In this paper we concentrate on this problem and theoretically investigate SPP and light scattering by individual silicon NPs located on a metal (gold) substrate and supporting ED and MD resonances in the visible spectral range. It is predicted and numerically demonstrated that, due to NP interaction

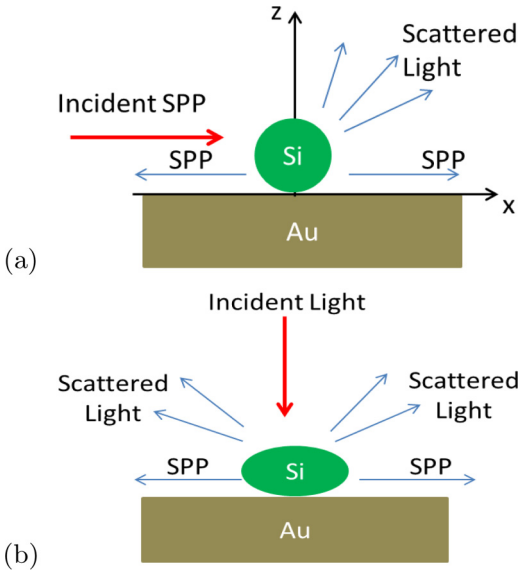

FIG. 1. (Color online) Schematic presentation of (a) SPP and (b) light scattering processes by an individual silicon NP located on a gold substrate. Scattering channels include the SPP excitation and scattering into light propagating away from the substrate.

with the electromagnetic fields reflected from the substrate (bianisotropy effect), the resonant unidirectional (forward) and elastic scattering of SPPs by spheroid silicon NPs can be realized within a narrow spectral range and exploited for developing new SPP-based photonic components and metasurfaces.

II. THEORETICAL BACKGROUND

We assume that a silicon NP is located near a metal surface supporting the SPP propagation (Fig. 1). This implies that dielectric permittivity ε_s of metal satisfies the conditions $-\mathrm{Re}(\varepsilon_s) > \varepsilon_d > 0$ and $-\mathrm{Re}(\varepsilon_s) \gg \mathrm{Im}(\varepsilon_s)$ in the considered spectral range, where ε_d is the dielectric permittivity of a medium above the metal surface (in this paper $\varepsilon_d = 1$). The last inequality guaranties that the SPP propagation length is larger than the SPP wavelength. Under these conditions, for the sake of simplicity, we can neglect the imaginary part of ε_s for calculations of extinction and scattering cross sections [32,33] (see also a remark at the beginning of Sec. III).

When an NP is illuminated either by an SPP wave propagating along the substrate surface or a light wave incident on the substrate, there are two scattering channels: (i) into SPPs and (ii) into light propagating away from the metal surface (Fig. 1). The scattered electric field above the surface ($z > 0$, Fig. 1) is

$$\mathbf{E}_a(\mathbf{r}) = \mathbf{E}_d(\mathbf{r}) + \mathbf{E}_r(\mathbf{r}) + \mathbf{E}_{\mathrm{SPP}}(\mathbf{r}), \tag{1}$$

where $\mathbf{E}_d(\mathbf{r})$ and $\mathbf{E}_r(\mathbf{r})$ are the electric fields of direct light waves and light reflected from the metal surface, respectively, and $\mathbf{E}_{\mathrm{SPP}}(\mathbf{r})$ is the field of the scattered SPPs. Applying the procedure of multipole decomposition in the far-field approximation for monochromatic electromagnetic waves (with the time dependence defined by $\exp(-i\omega t)$, where ω is the angular frequency), the electric field $\mathbf{E}_{\mathrm{scat}}$ of scattered waves can be expressed in the following general form [33]:

$$\mathbf{E}_{\mathrm{scat}}(\mathbf{r}) \approx \frac{k_0^2 e^{-ik\mathbf{n}\cdot\mathbf{r}_0}}{\varepsilon_0}\hat{S}(\mathbf{r})\Big\{\mathbf{p} - \frac{k}{\omega}[\mathbf{n}\times\mathbf{m}] - \frac{ik}{6}\hat{Q}\mathbf{n} - \frac{k^2}{6}\hat{O}(\mathbf{nn}) + \frac{ik^2}{2\omega}[\mathbf{n}\times\hat{M}\mathbf{n}]\Big\}, \tag{2}$$

where k_0 is the wave number of light; ε_0 is the vacuum dielectric permittivity; $\mathbf{p}$ and $\mathbf{m}$ are the electric and MD moments of the scatterer, respectively; $\hat{Q}$ and $\hat{M}$ are the electric and magnetic quadrupole tensors of the scatterer, respectively; and $\hat{O}$ is the electric octupole tensor. The multipole moments are calculated (and consequently located) at the point $\mathbf{r}_0$. The value k, vector $\mathbf{n}$, and tensor $\hat{S}(\mathbf{r})$ are determined by the scattered waves [Eq. (1)]. For $\mathbf{E}_d(\mathbf{r})$, $k = k_d = k_0\sqrt{\varepsilon_d}$ and $\mathbf{n} = \mathbf{r}/|\mathbf{r}|$. For $\mathbf{E}_r(\mathbf{r})$, $k = k_d = k_0\sqrt{\varepsilon_d}$ and $\mathbf{n} = \mathbf{r}'/|\mathbf{r}'|$, where $\mathbf{r}' = (x,y,-z)$. For $\mathbf{E}_{\mathrm{SPP}}(\mathbf{r})$, $k = k_S = k_0\sqrt{\varepsilon_s\varepsilon_d/(\varepsilon_s+\varepsilon_d)}$, $\mathbf{n} = (x/\rho, y/\rho, -ia)$, $\rho = \sqrt{x^2+y^2}$, and $a = \sqrt{-\varepsilon_d/\varepsilon_s}$. The multipole moments of the NP are calculated using the induced polarization $\mathbf{P}(\mathbf{r}) = \varepsilon_0(\varepsilon_p - \varepsilon_d)\mathbf{E}(\mathbf{r})$ inside the NP, where $\mathbf{E}(\mathbf{r})$ is the total electric field inside the NP and ε_p is its dielectric permittivity:

$$\mathbf{p} = \int_{V_S}\mathbf{P}(\mathbf{r}')d\mathbf{r}' \tag{3}$$

is the ED moment;

$$\hat{Q} \equiv \hat{Q}(\mathbf{r}_0) = 3\int_{V_S}(\Delta\mathbf{r}\mathbf{P}(\mathbf{r}') + \mathbf{P}(\mathbf{r}')\Delta\mathbf{r})d\mathbf{r}', \tag{4}$$

$$\mathbf{m} \equiv \mathbf{m}(\mathbf{r}_0) = -\frac{i\omega}{2}\int_{V_S}[\Delta\mathbf{r}\times\mathbf{P}(\mathbf{r}')]d\mathbf{r}' \tag{5}$$

are the electric quadrupole tensor and the MD moment, where V_S is the NP's volume; $\Delta\mathbf{r} = \mathbf{r}' - \mathbf{r}_0$ (it is convenient to choose the point $\mathbf{r}_0$ at the NP's center of mass [23]). Note that $\mathbf{nn}$ and $\Delta\mathbf{r}\mathbf{P}$ represent the dyadic (outer) products between the corresponding vectors. Expressions for higher-order multipole moments and electric fields generated (scattered) by the corresponding multipole moments can be found elsewhere [33].

Scattering and extinction cross sections

Let us first consider the scattering cross sections. Since scattered light waves propagate away from the metal surface, their interference with scattered SPP waves propagating along the surface is negligible in the far-field zone. As a result the total scattering cross section σ_{scat} can be represented as the sum of two parts σ_{SPP} and σ_{Light} corresponding to the scattering into SPP and into light propagating away from the surface, respectively [12,32]:

$$\sigma_{\mathrm{SPP}} = \frac{P_{\mathrm{SPP}}}{P_{\mathrm{in}}} \quad \text{and} \quad \sigma_{\mathrm{Light}} = \frac{P_{\mathrm{L}}}{P_{\mathrm{in}}}, \tag{6}$$

where P_{SPP} and P_{L} are the scattered powers into SPP and light, respectively, and P_{in} is the incident wave power. For the incidence of a light plane wave, $P_{\mathrm{in}} = \sqrt{\varepsilon_0\varepsilon_d/\mu_0}|\mathbf{E}_0|^2/2$, and in the case of an incident SPP plane wave

$$P_{\mathrm{in}} = \frac{1}{2k_0}\sqrt{\frac{\varepsilon_0}{\mu_0}}\frac{1-a^2}{2a}(1-a^4)\left|\mathbf{E}_0^{\mathrm{SPP}}\right|^2,$$

where $\mathbf{E}_0$ and $\mathbf{E}_0^{\mathrm{SPP}}$ are the electric amplitudes of the incident light plane wave and the normal (out-of-plane) component of the incident SPP plane wave, respectively. Note that, in the case of SPP incidence, P_{in} is determined per unit length [12,15].

The power of a scattered SPP propagating into an in-plane angle $[\varphi,\varphi+d\varphi]$ (the polar coordinate system) is given by the expression [33]

$$P(\varphi)d\varphi = \sqrt{\frac{\varepsilon_0}{\mu_0}}\frac{(1-a^2)(1-a^4)}{4ak_0}|E_{\mathrm{SPP}z}|^2\rho d\varphi, \qquad (7)$$

where the z component (out of plane) of the scattered SPP electric field $E_{\mathrm{SPP}z}$ is taken in the domain above the metal surface just on the metal surface ($z=0$). Note that the expression (7) was obtained by neglecting the imaginary part of metal permittivity ε_s. The total SPP power can be written down as follows:

$$P_{\mathrm{SPP}} = \int_0^{2\pi} P(\varphi)d\varphi = \int_{-\pi/2}^{\pi/2} P(\varphi)d\varphi + \int_{\pi/2}^{3\pi/2} P(\varphi)d\varphi, \qquad (8)$$

where the first and second integrals from the right-hand side are the "forward" F_{SPP} and "backward" B_{SPP} scattering powers, respectively [here we suppose that the incident SPP plane wave propagates along the positive direction of the x axis as shown in Fig. 1(a)].

Using the electric field $E_{\mathrm{SPP}z}$ as a superposition of multipole fields (2), the contribution of different multipoles in the scattered SPP power can be evaluated. In the electric and MD approximation one can write [33]

$$E_{\mathrm{SPP}z} \sim p_z + iap_\rho - (1-a^2)\sqrt{\mu_0\varepsilon_0}\,\frac{k_S}{k_0}\,m_\varphi, \qquad (9)$$

where p_z and p_ρ are the out-of-plane and in-plane components of ED moment $\mathbf{p}$, respectively, and m_φ is the in-plane component of the MD moment $\mathbf{m}$. The in-plane components are connected with the Cartesian component of the corresponding dipole moments: $p_\rho = p_x\cos\varphi + p_y\sin\varphi$ and $m_\varphi = -m_x\sin\varphi + m_y\cos\varphi$. It is important to note that (i) the contribution of the in-plane component of ED moment p_ρ is proportional to the parameter a, which is very small ($a \ll 1$) in the spectral region where SPPs can be excited; and (ii) the out-of-plane component m_z of MD does not excite the SPP on metal surfaces.

The scattered power into the light waves propagating away from the metal surface can be calculated from [33]

$$P_{\mathrm{L}} = \frac{1}{2}\sqrt{\frac{\varepsilon_0\varepsilon_d}{\mu_0}}\int_0^{\pi/2}\int_0^{2\pi}|\mathbf{E}_d+\mathbf{E}_r|^2r^2\sin\theta\,\mathrm{d}\theta\mathrm{d}\varphi, \qquad (10)$$

where φ and θ are the azimuthal and polar angles of the spherical coordinate system, respectively. Note that the expression

$$\sigma(\varphi,\theta) = \frac{1}{2P_{\mathrm{in}}}\sqrt{\frac{\varepsilon_0\varepsilon_d}{\mu_0}}|\mathbf{E}_d+\mathbf{E}_r|^2r^2 \qquad (11)$$

is the differential cross section of the scattering into the light propagating away from the substrate surface. This value describes the angular distribution of the scattered light. In the electric and MD approximation one can write [33]

$$(\mathbf{E}_d+\mathbf{E}_r)_\varphi \sim [r^{(s)}e^{ik_d2z_0\cos\theta}+1](p_\varphi+\sqrt{\mu_0\varepsilon_0\varepsilon_d}\,m_z\sin\theta) + [r^{(s)}e^{ik_d2z_0\cos\theta}-1]\sqrt{\mu_0\varepsilon_0\varepsilon_d}\,m_\rho\cos\theta, \qquad (12)$$

and

$$(\mathbf{E}_d+\mathbf{E}_r)_\theta \sim [r^{(p)}e^{ik_d2z_0\cos\theta}+1](\sqrt{\mu_0\varepsilon_0\varepsilon_d}\,m_\varphi-p_z\sin\theta) + [1-r^{(p)}e^{ik_d2z_0\cos\theta}]\,p_\rho\cos\theta, \qquad (13)$$

where $r^{(s)}$ and $r^{(p)}$ are the reflection coefficients for s- and p-polarized waves, respectively [33], z_0 is the position of the dipole moments, and p_ρ and $p_\varphi = -p_x\sin\varphi + p_y\cos\varphi$ are the in-plane components of the particle ED moment, $m_\rho = m_x\cos\varphi + m_y\sin\varphi$. In contrast to Eq. (9) contributions of the ED in-plane components in the electric field [Eqs. (12) and (13)] are not proportional to the small parameter a.

The extinction (scattering and absorption) cross section σ_{ext} can be evaluated by [11,34]

$$\sigma_{\mathrm{ext}} = \frac{P_{\mathrm{ext}}}{P_{\mathrm{in}}} = \frac{\omega}{2P_{\mathrm{in}}}\,\mathrm{Im}\int_{V_S}\mathbf{E}_0^*(\mathbf{r})\cdot\mathbf{P}(\mathbf{r})d\mathbf{r}, \qquad (14)$$

where P_{ext} is the extinction power and $\mathbf{E}_0(\mathbf{r})$ is the electric field of the incident (external) electromagnetic waves (the field that we would have if the scattering object was not there). The multipole decomposition of the extinction cross section is presented elsewhere [33]. In the case of SPP plane-wave incidence [Fig. 1(a)],

$$\mathbf{E}_0(\mathbf{r}) = E^{\mathrm{SPP}}e^{ik_Sx-ak_Sz}(-ia\hat{x},0,\hat{z}), \quad z>0, \qquad (15)$$

where E^{SPP} is the amplitude magnitude of the electric field. In the case of light plane-wave incidence,

$$\mathbf{E}_0(\mathbf{r}) = e^{ik_dx\sin\beta}\left(\mathbf{E}_0^{\mathrm{in}}e^{-ik_dz\cos\beta}+R\mathbf{E}_0^{\mathrm{ref}}e^{ik_dz\cos\beta}\right), \qquad (16)$$

where β is the incident angle; $\mathbf{E}_0^{\mathrm{in}}$ and $\mathbf{E}_0^{\mathrm{ref}}$ are the amplitude vectors of the incident and reflected waves, respectively; and R is the reflection coefficient depending on the wave polarization. Here we suppose that the light incident plane is the xz plane [Fig. 1(b)]. In the case of TE polarization $\mathbf{E}_0^{\mathrm{in}} = \mathbf{E}_0^{\mathrm{ref}}$ and

$$R = \frac{\cos\beta-\sqrt{(\varepsilon_s/\varepsilon_d)-\sin^2\beta}}{\cos\beta+\sqrt{(\varepsilon_s/\varepsilon_d)-\sin^2\beta}}.$$

In the case of TM polarization $E_{0x}^{\mathrm{in}} = -E_{0x}^{\mathrm{ref}}$ and $E_{0z}^{\mathrm{in}} = E_{0z}^{\mathrm{ref}}$, and

$$R = \frac{\varepsilon_s\cos\beta-\varepsilon_d\sqrt{(\varepsilon_s/\varepsilon_d)-\sin^2\beta}}{\varepsilon_s\cos\beta+\varepsilon_d\sqrt{(\varepsilon_s/\varepsilon_d)-\sin^2\beta}}.$$

The magnetic field $\mathbf{H}_0$ can be found using the Maxwell equation $\nabla\times\mathbf{E}_0 = ik_0\sqrt{\mu_0/\varepsilon_0}\mathbf{H}_0$.

III. RESULTS AND DISCUSSIONS

Our numerical calculations are carried out using the discrete dipole approximation (DDA) [34] including the procedure of the multipole decomposition [33]. We consider first a spherical 95-nm-radius silicon NP placed near a gold surface (the space gap between the NP and the substrate is equal to 5 nm). The studied system together with the chosen coordinate system are

shown in Fig. 1(a). Dielectric constants for gold and crystalline silicon are taken from the tables in Refs. [35,36], respectively. Importantly, for gold $\mathrm{Re}\, a \gg \mathrm{Im}\, a$ and $a \approx \mathrm{Re}\, a \leqslant 0.3$ and $k_S/k_0 \approx \mathrm{Re}\, k_S/k_0 \approx 1$ in the considered optical range. This will be used in the following when conducting estimations. Note that in our approach the calculation of extinction and scattering sections is divided on two steps. First, the electric field inside NPs and corresponding multipole moments are calculated. Second the scattered fields in the far-field zone and the scattering cross sections are calculated. In the first step we take into account the imaginary part of the metal dielectric constant. Due to the dressing and bianisotropic effects [12,37] the calculated dipole (multipole) moments include influence of this imaginary part. As a result the extinction cross sections include the substrate influence on the SPP or light absorption in the NPs.

A. SPP scattering

Scattering and extinction cross sections for the case of SPP scattering by the spherical silicon NP are shown in Fig. 2(a). Small differences between the scattering and extinction cross sections indicate very weak absorption of electromagnetic energy by the NP. The partial scattering cross sections for the two scattering channels are also presented in Fig. 2(a). In the whole considered spectral range, the (elastic) SPP scattering into SPPs is more efficient than the (inelastic) SPP scattering into light. Especially, this concerns the spectral vicinity of the wavelength of 645 nm, at which the ratio between σ_{SPP} and σ_{Light} is at its maximum and equals to 4 [blue curve in Fig. 2(b)]. Note that this maximum of the elastic SPP scattering is realized outside the resonance of the total scattering cross section and outside the spectral region, within which the forward SPP-into-SPP scattering dominates over the backward one, resulting in the unidirectional SPP scattering [red curve in Fig. 2(b)]. For physical clarification of these scattering features, we employ a multipole analysis of SPP scattering by NPs on a plane surface [33]. From the multipole decomposition presented in Fig. 3 one can see that the extinction is basically determined by contributions of the out-of-plane ED (p_z) and in-plane MD (m_y) moments of the NP. Contributions of the in-plane ED (p_x) and electric quadrupole moments in the extinction cross section are weak. The broad peak is associated with resonant excitation of m_y at the wavelength of 670 nm and the nonresonant contribution from p_z. Thus the resonant forward (unidirectional) scattering of the incident SPP into SPPs [Fig. 2(b)] is explained by the interference effect between electromagnetic fields generated by m_y and p_z. From Eq. (9) neglecting contribution of ap_x and taking into account that $a^2 \ll 1$ and $k_S/k_0 \approx 1$ one can write

$$E_{\mathrm{SPP}z} \sim p_z - \sqrt{\mu_0\varepsilon_0}\, m_y \cos\varphi. \tag{17}$$

At the condition of the forward (backward) scattering (with respect to the direction of the incident SPP) $\varphi = 0(\pi)$. Therefore the ratio between the elastic forward and backward SPP scattering can be estimated as

$$\frac{|p_z - \sqrt{\mu_0\varepsilon_0}\, m_y|^2}{|p_z + \sqrt{\mu_0\varepsilon_0}\, m_y|^2}. \tag{18}$$

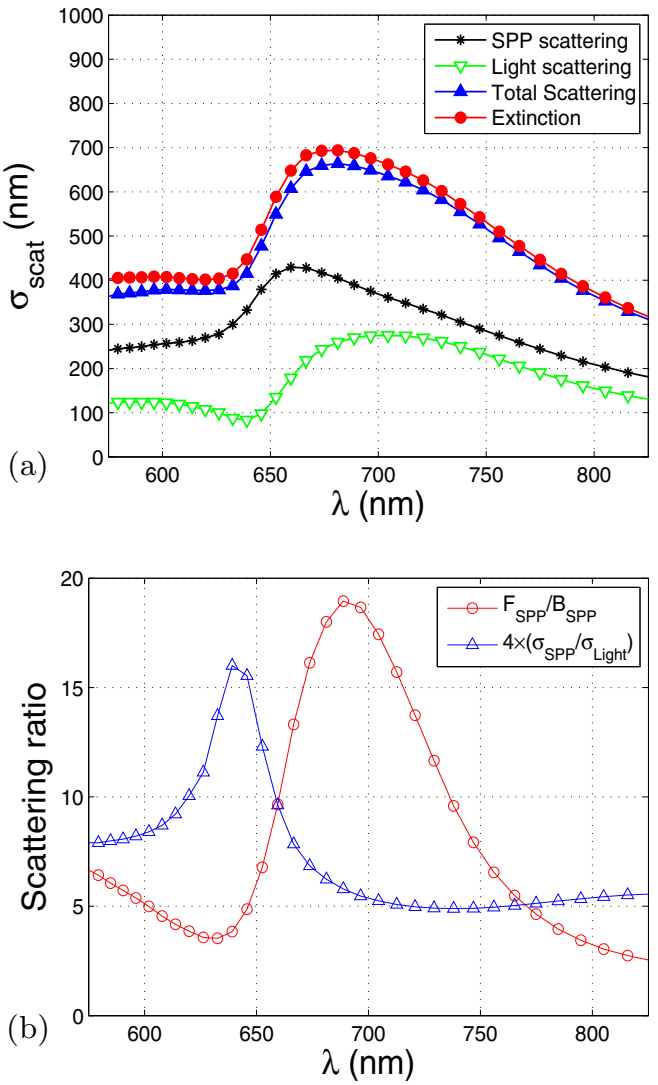

FIG. 2. (Color online) (a) Extinction and scattering cross-section spectra of a spherical silicon NP (with the radius of 95 nm) located on a gold surface and irradiated by a SPP plane wave. SPP (Light) scattering corresponds to σ_{SPP} (σ_{Light}). (b) Corresponding spectral dependence of the ratios $\sigma_{\mathrm{SPP}}/\sigma_{\mathrm{Light}}$ and $F_{\mathrm{SPP}}/B_{\mathrm{SPP}}$. For convenient presentation the ratio $\sigma_{\mathrm{SPP}}/\sigma_{\mathrm{Light}}$ was multiplied by the factor 4.

The spectral maximum of the ratio (18) shown in Fig. 4 is in good agreement with the corresponding maximum for $\mathrm{F_{SPP}/B_{SPP}}$ in Fig. 2(b), confirming a very small role of the p_x component in the unidirectional SPP scattering.

Weak negative (antiresonant) contribution of the in-plane ED p_x into the extinction cross section (Fig. 3, $\lambda = 650$ nm) is due to the bianisotropic effect, where the ED response is induced mainly by the electric field generated by the MD and reflected from the metal substrate surface. This is a reason why this antiresonance appears at the condition of the MD resonance and the induced in-plane ED moment is out of phase with the external incident electric field. Generally, the bianisotropic effect can be perceived as an excitation of the in-plane electric (magnetic) dipole moment by the magnetic (electric) field of incident electromagnetic waves [37]. In this case the in-plane components of electric $\mathbf{p}_{||} = (p_x, p_y)$ and

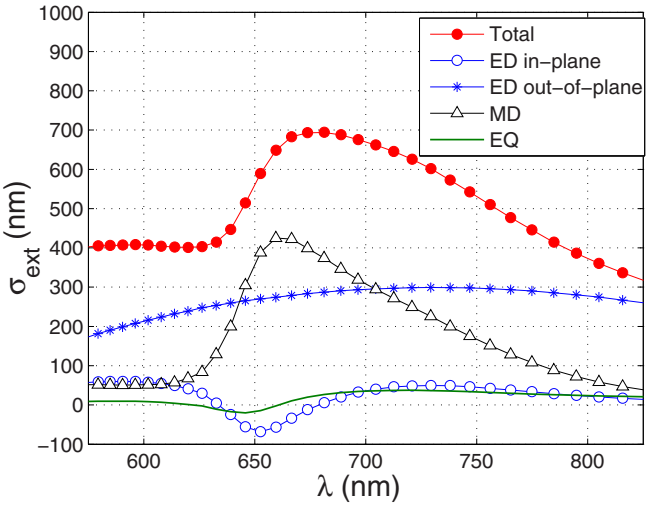

FIG. 3. (Color online) Extinction cross-section spectra of a spherical silicon NP (with the radius of 95 nm) located on a gold surface. The plot shows different multipole contributions to the total extinction cross section: ED, electric dipole; MD, magnetic dipole; EQ, electric quadrupole.

magnetic $\mathbf{m}_{||} = (m_x, m_y)$ dipole moments are determined by the expressions

$$\mathbf{p}_{||} = \hat{\alpha}_e \mathbf{E}_0 + \hat{\alpha}_{eh} \mathbf{H}_0, \tag{19}$$

$$\mathbf{m}_{||} = \hat{\alpha}_h \mathbf{H}_0 + \hat{\alpha}_{he} \mathbf{E}_0, \tag{20}$$

where the tensors $\hat{\alpha}_{eh}$ and $\hat{\alpha}_{he}$ provide the bianisotropy effect and the direct polarizability tensors $\hat{\alpha}_e$ and $\hat{\alpha}_h$ depend on the electromagnetic interaction between the NP and substrate. Moreover $\hat{\alpha}_{eh} = \mu_0 \hat{\alpha}_{he}$ [37].

In the spectral region corresponding to the p_x antiresonance the magnitudes of p_x and p_z are close to each other (Fig. 5). Therefore both ED components and the MD will determine the scattered light waves [Eqs. (12) and (13)]. However, due to the bianisotropic effect, the scattered electric field generated by p_x

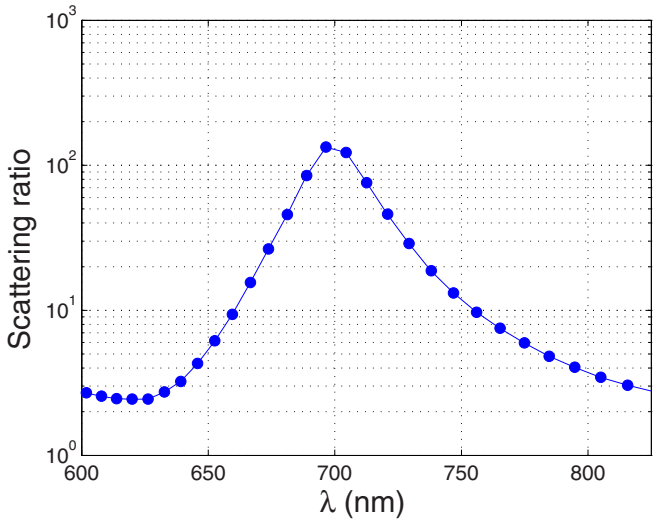

FIG. 4. (Color online) Spectral dependence of the ratio (18) for the parameters as in Fig. 2.

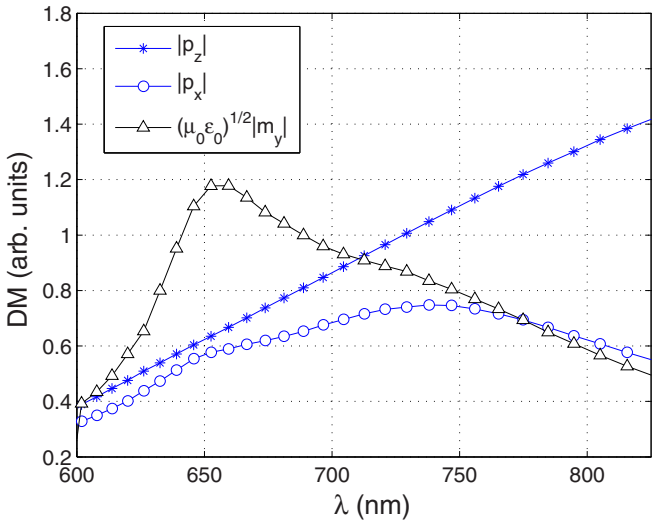

FIG. 5. (Color online) The magnitudes of the in-plane p_x and out-of-plane p_z components of the ED moment and the in-plane m_y component of the MD moment of spherical silicon NP irradiated by a SPP plane wave. The parameters are as in Fig. 2.

will be out of phase with respect to the electric field generated by m_y. As a result the scattered light waves propagating away from the surface will be partially suppressed, providing the minimum of σ_{Light} [Fig. 2(a)] and the maximum for the ratio $\sigma_{\text{SPP}}/\sigma_{\text{Light}}$ [Fig. 2(b)]. Thus the spectral difference between the two resonances presented in Fig. 2(b) is explained (i) by different importance of the in-plane component p_x in the two scattering channels and (ii) by the bianisotropic effect.

In order to realize the resonant unidirectional and elastic SPP scattering within the same spectral region, one has to increase the contribution of the in-plane component p_x into the elastic SPP scattering. Here, we suggest achieving this effect by reshaping spherical particles into oblate spheroids. It is seen (Fig. 6) that different aspect ratios q ($q = 1$ corresponds to spherical shape; for oblate spheroids $q > 1$) result in different magnitudes of the dipole components p_x, p_z, and m_y excited by SPP plane waves in silicon oblate spheroids. Note that the considered NPs have the same volume, corresponding to a sphere with the radius of 95 nm. With increasing of the oblation parameters q the magnitude of the in-plane dipole component p_x grows, including the two resonances [Fig. 6(b)]. The other (out-of-plane) dipole component p_z is decreased with increasing q [Fig. 6(a)], providing more important influence of p_x on the SPP scattering in the case of oblate NPs. Note that the two resonances of p_x ($q = 1.8$) appear at the spectral regions where the corresponding resonances of m_y are also excited [Figs. 6(b) and 6(c)]. This correlation is a result of the bianisotropy effect connecting the electric and MD resonances. The spectral shifts of the p_x and m_y resonances with changing of q are a result of complex combination of the bianisotropy and dressing effects. The latter can be illustrated using the image theory. For more oblate spheroid NPs the distance between induced dipoles and their images (with respect to the metal-mirror surface) is decreased, providing stronger interaction between them. As a result the in-plane MD (ED) resonance could have blueshift (redshift) because the MD (ED)

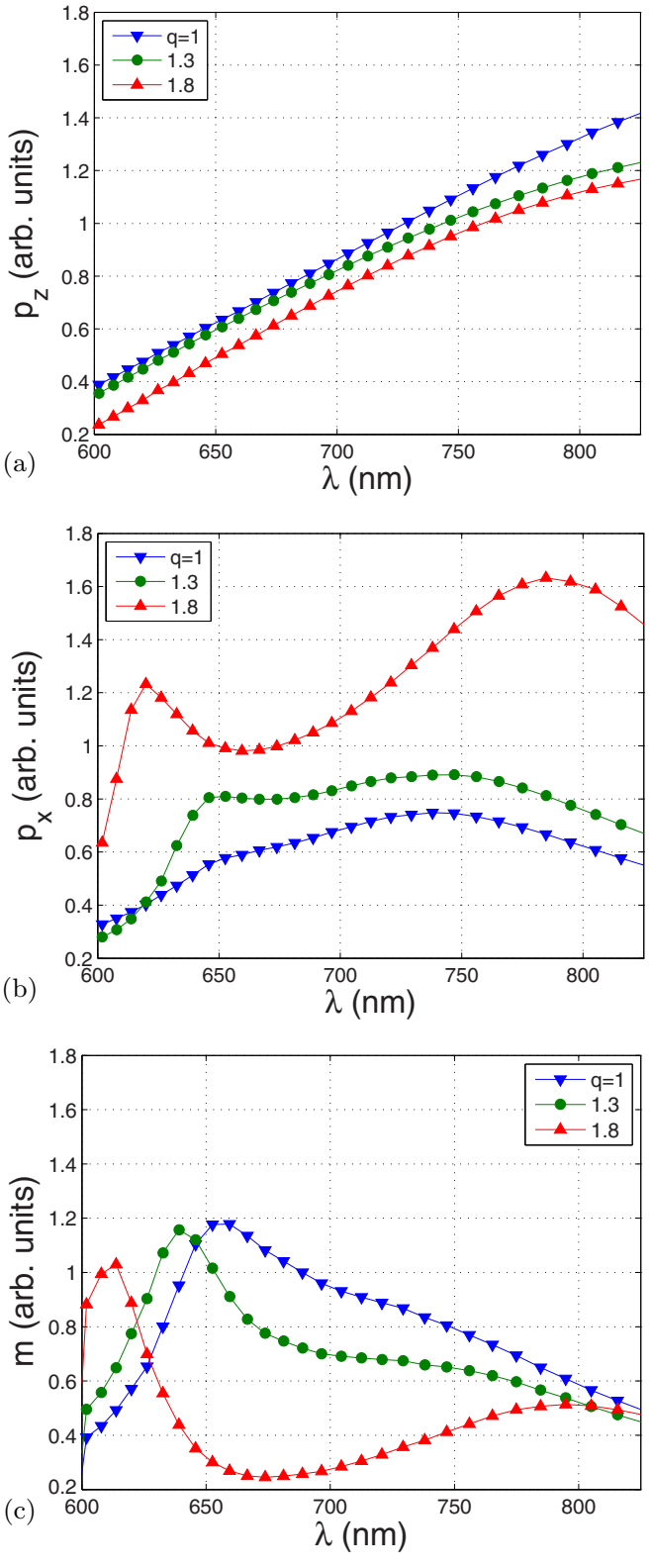

FIG. 6. (Color online) The magnitudes of the (a) out-of-plane p_z and (b) in-plane p_x components of the ED moment and (c) the in-plane m_y component of the MD moment of spheroid silicon NPs irradiated by a SPP plane wave. q is the NP aspect ratio. The volumes of the NPs are corresponded to a spherical NP with the radius of 95 nm.

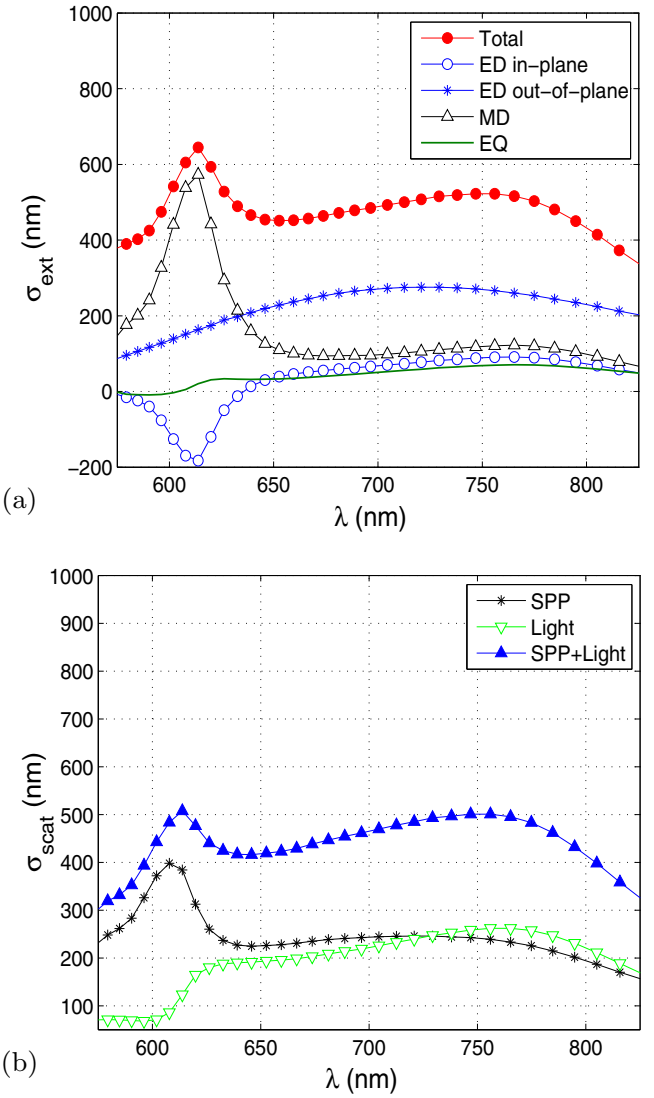

FIG. 7. (Color online) (a) Extinction cross-section spectra of an oblate spheroid silicon NP (the aspect ratio $q = 1.8$; the volume corresponds to a spherical NP with the radius of 95 nm) located on a gold surface and irradiated by a SPP plane wave. The plot shows different multipole contributions to the total extinction cross section: ED, electric dipole; MD, magnetic dipole; EQ, electric quadrupole. (b) Scattering cross-section spectra of this spheroid silicon NP. SPP (Light) corresponds to σ_{SPP} (σ_{Light}).

and its image are directed in the same (opposite) directions [38].

Thus the two resonances and the spectral difference between them shown in Figs. 6(b) and 6(c) for the oblate spheroid NP with $q = 1.8$ explaining the spectral features of the extinction and scattering cross sections presented in Fig. 7. The multipole decomposition in Fig. 7(a) confirms that the extinction and scattering cross sections are determined by the electric and MD modes excited by SPP waves inside the oblate NP. In contrast to the results shown in Fig. 3 for the spherical NP the negative contribution of the p_x term into the short-wavelength resonance of the total extinction cross

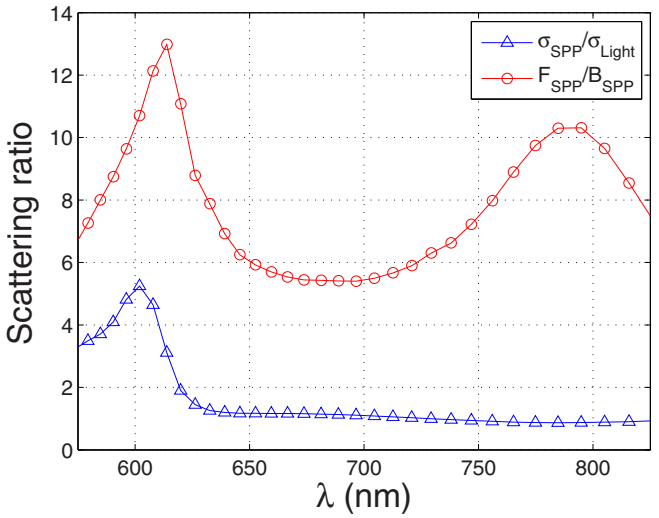

FIG. 8. (Color online) Spectral dependence of the ratios $\sigma_{SPP}/\sigma_{Light}$ and F_{SPP}/F_{Light} for the spheroid silicon NP irradiated by a SPP plane wave. The parameters are as in Fig. 9.

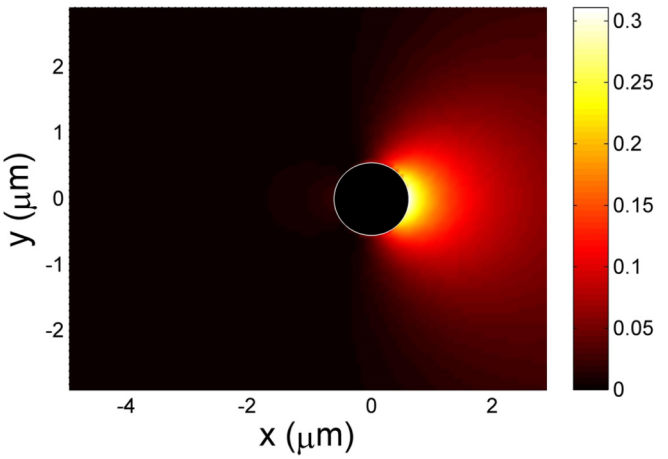

FIG. 9. (Color online) Scattered SPP electric-field intensity (arb. units) calculated 150 nm above the air-gold interface for the SPP plane wave (light wavelength 614 nm) being incident on the oblate spheroid silicon NP ($q = 1.8$). The black circles indicate the NP position.

section in Fig. 7(a) is increased, indicating on importance of the in-plane p_x component in the SPP scattering. As a result the elastic SPP scattering maximum ($\sigma_{SPP}/\sigma_{Light}$) and the maximum of the SPP forward scattering (F_{SPP}/B_{SPP}) are realized at the narrow spectral region around $\lambda = 610$ nm (Fig. 8). It is seen from the figure that under these conditions the SPP forward (SPP elastic) scattering is ten (five) times more effective than the SPP backward (SPP into light) scattering. The resonance of F_{SPP}/B_{SPP} at $\lambda = 790$ nm in Fig. 8 is realized when $\sigma_{SPP}/\sigma_{Light} \simeq 1$.

For the explicit demonstration of the SPP backward scattering suppression, we calculated the SPP intensity distribution in a plane located in the near-field zone above the metal substrate surface with the oblate NP ($q = 1.8$) illuminated by an incident SPP wave corresponding to the resonant wavelength $\lambda = 614$ nm. The spatial intensity distribution of the scattered SPP demonstrates close to complete suppression of the SPP backward scattering (Fig. 9). Moreover, the SPP-into-light scattering is also significantly weakened at this resonant wavelength (Fig. 10). Concluding this subsection, we note that, if a space gap between the oblate NPs and metal substrate surface increases, the spectral distribution of the SPP scattering cross section begins to look like that of the scattering cross section for spherical NPs located on the substrate surface.

B. Light scattering

Let us consider the reciprocal light scattering from silicon NPs located on a gold surface and having parameters as in the previous subsection. Here we assume a normal incidence of linear-polarized light plane waves as it is shown in Fig. 1(b). The spectra of extinction cross sections for spherical and oblate spheroid NPs are presented in Fig. 11. From the multipole decompositions included there it is clear that the optical properties of the NPs are determined by solely their electric and MD moments. Due to the bianisotropy effect both resonant peaks of the extinction cross sections in Figs. 11(a) and 11(b) correspond to the simultaneous resonant excitation of the electric and MD moments. In contrast to the case of the SPP scattering here the partial negative contribution in total extinction cross sections corresponds to the MD term (MD) of the multipole decomposition (Fig. 11). That results from different space distributions of the electric and magnetic fields of the incident SPP and light waves near a metal surface. Note that the NP MD moment is not in phase with the magnetic field of the incident light waves at the spectral region where the MD contribution in the extinction cross section is negative. Another important difference from the case of SPP scattering is the absence of the out-of-plane component p_z under the condition of normal light incidence. Consequently, Eq. (9) reduces to the following one:

$$E_{SPPz} \sim (iap_x - (1 - a^2)\sqrt{\mu_0\varepsilon_0}\, m_y)\cos\varphi \qquad (21)$$

for the incident light polarized along the x axis. As a result, we obtain the condition for the suppression of SPP excitation

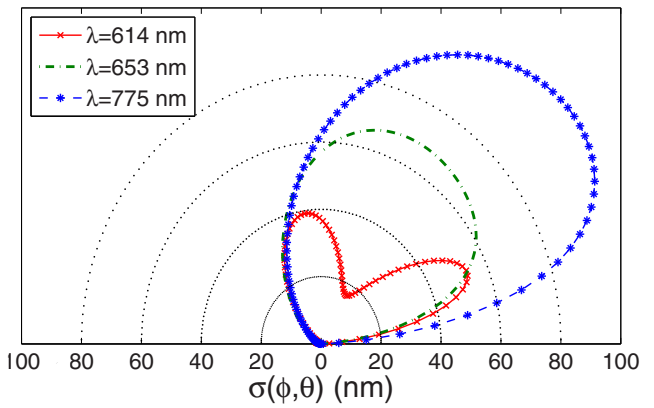

FIG. 10. (Color online) Differential scattering cross sections (scattering diagrams) of SPP-into-light scattering by the oblate spheroid silicon NP ($q = 1.8$) calculated in the xz plane.

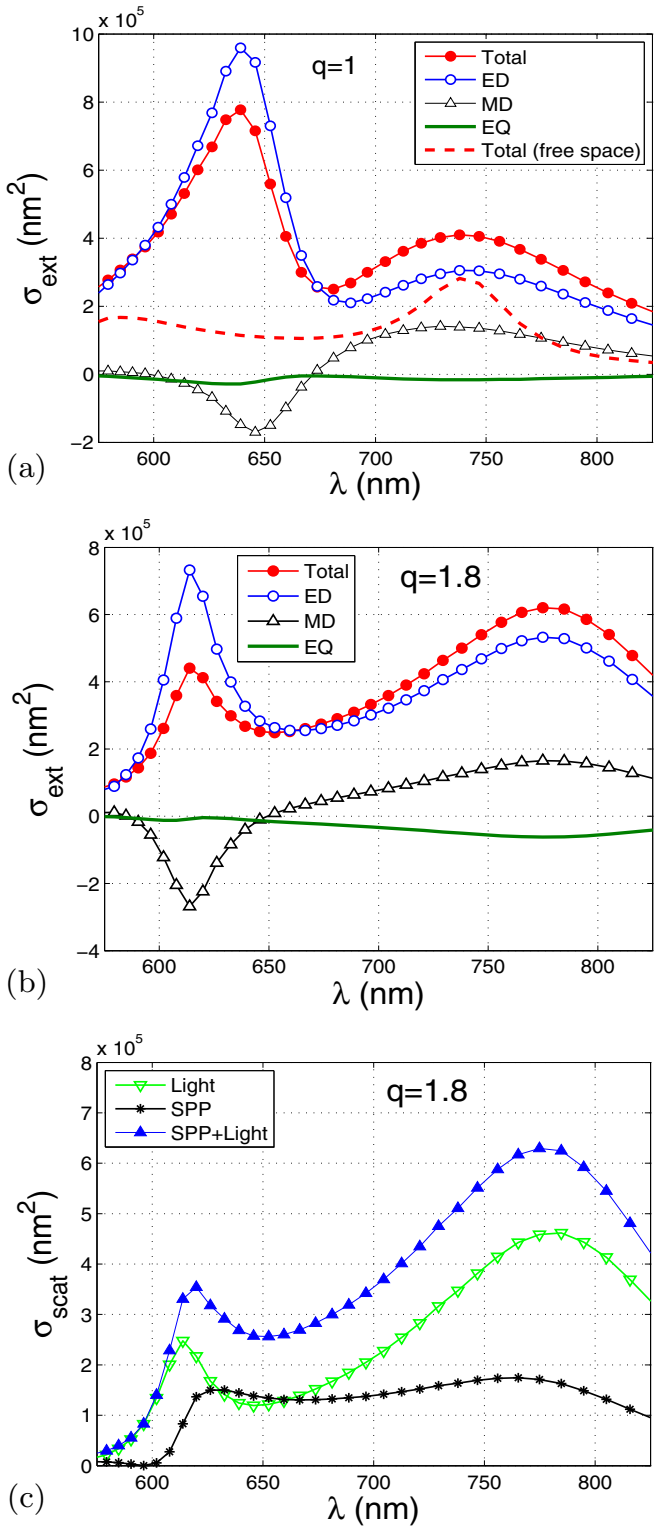

FIG. 11. (Color online) Extinction cross-section spectra of (a) spherical and (b) oblate spheroid silicon NPs (q is the aspect ratio; the volumes correspond to a spherical NP with the radius of 95 nm) located on a gold surface and irradiated by a normally incident light plane wave. The plot shows different multipole contributions to the total extinction cross section. (c) Scattering cross-section spectra of the same spheroid silicon NP. SPP (Light) corresponds to σ_{SPP} (σ_{Light}). For the sake of comparison the extinction cross sections of the NPs without substrates have been added in (a).

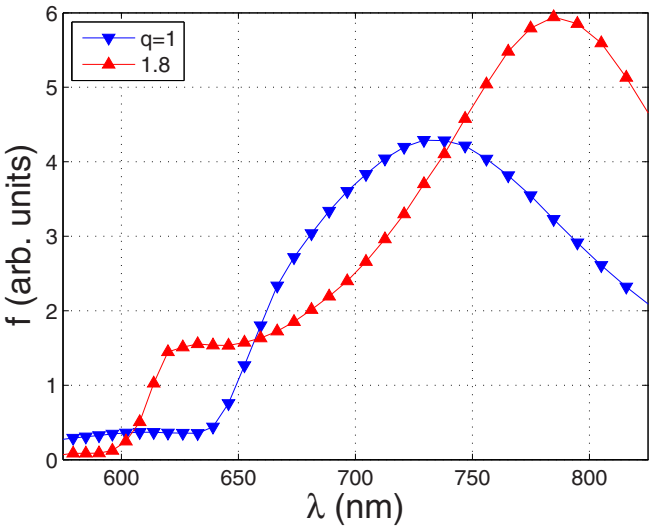

FIG. 12. (Color online) Spectral dependence of the function $f = |(iap_x - (1-a^2)\sqrt{\mu_0\varepsilon_0}\, m_y)|^2$ for the spherical and oblate spheroid silicon NPs, Eq. (21).

in the system

$$p_x \approx -\sqrt{\frac{\mu_0\varepsilon_0\varepsilon_s}{\varepsilon_d}}\, m_y, \tag{22}$$

where ε_s is the complex number and one takes $\sqrt{-1} = i$. Owing to the bianisotropy interaction existing only between the in-plane ED and MD components, the condition (22) could be satisfied in the spectral region, where resonances of the ED and MD contributions in the extinction spectrum have opposite signs. Indeed, one notices [Fig. 11(c)] that the scattering of light into the SPP is significantly suppressed in the spectral region below $\lambda = 600$ nm. Figure 12 demonstrates the spectral dependence of the expression $f = |(iap_x - (1-a^2)\sqrt{\mu_0\varepsilon_0}\, m_y)|^2$ from Eq. (21) for the spherical and spheroid NPs. In both cases the minimum (maximum) of excited SPPs

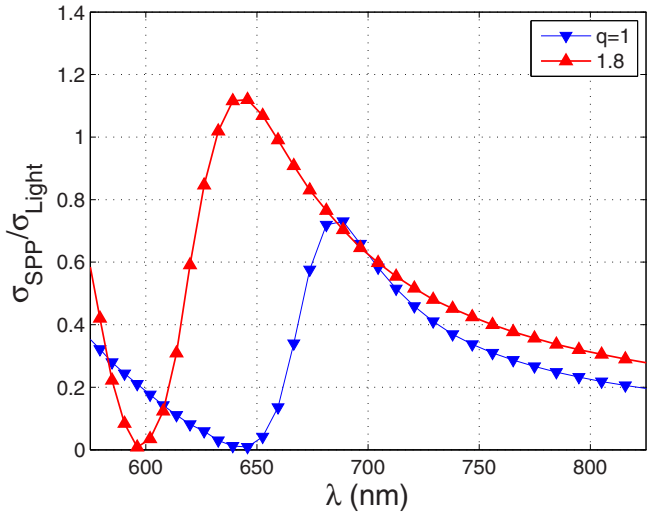

FIG. 13. (Color online) Spectral dependence of $\sigma_{\mathrm{SPP}}/\sigma_{\mathrm{Light}}$ calculated for the spherical and oblate spheroid silicon NPs irradiated by normal-incident light plane waves.

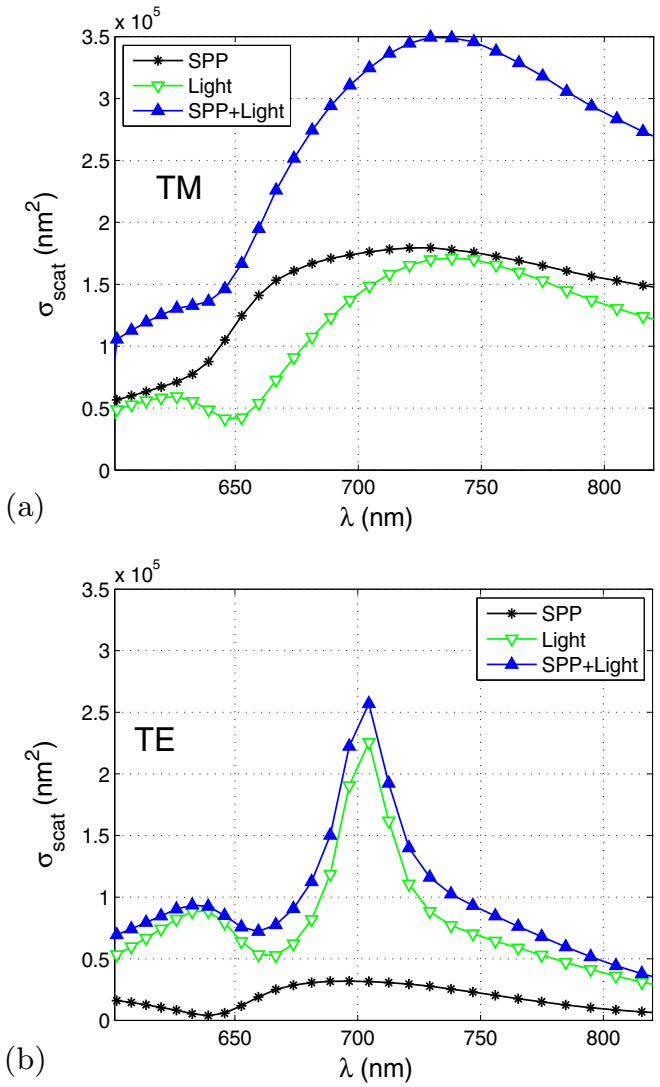

FIG. 14. (Color online) Scattering cross-section spectra of spherical silicon NPs with the radius of 95 nm located on a gold surface and irradiated by incline-incident light plane waves. The incident angle is equal to 70°. SPP (Light) corresponds to $\sigma_{\rm SPP}$ ($\sigma_{\rm Light}$).

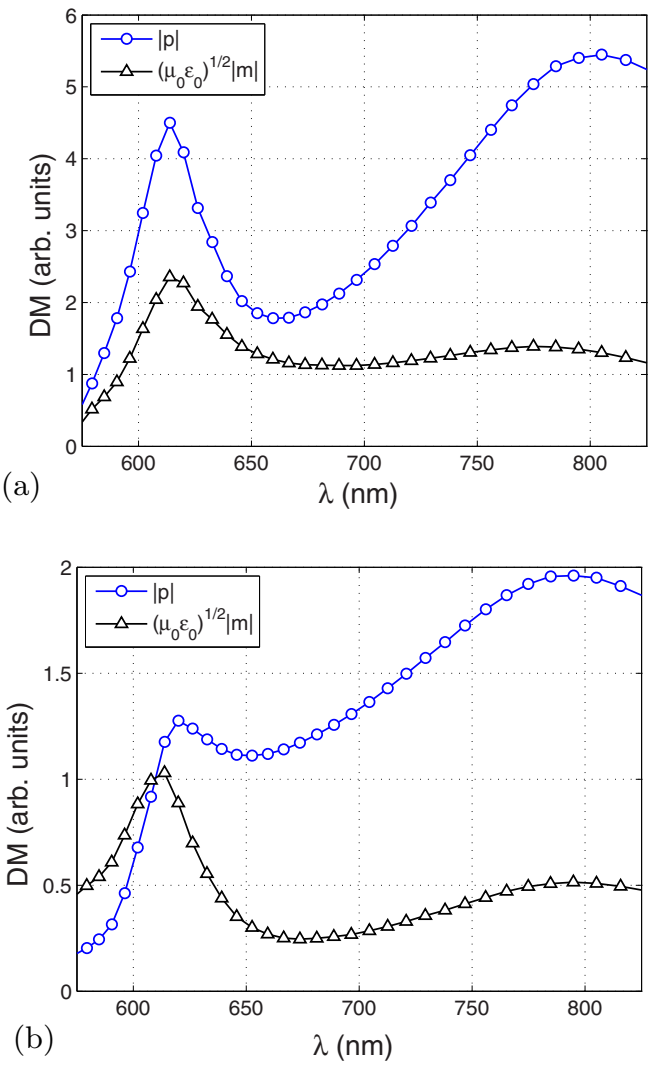

FIG. 15. (Color online) Magnitudes of the ED moment **p** and the MD moment $\sqrt{\mu_0\varepsilon_0}\,\mathbf{m}$ of a spheroidal silicon NP with $q = 1.8$ irradiated by (a) normal-incident light plane waves and (b) SPP plane waves. The NP volume corresponds to that of a spherical 95-nm-radius NP.

in the considered systems is realized at the condition of the short-wavelength (long-wavelength) resonance of the total extinction and scattering cross sections (Fig. 11). Importantly the SPP suppression is realized for silicon nanospheroids with different aspect ratios at the condition of the short-wavelength resonance because the NP electric and MD resonances are automatically adjusted to each other due to the strong bianisotropy effect. Changing the NP shape it is possible to shift the spectral point where the SPP excitation is suppressed (Fig. 13). Similar behavior can be also realized by changing the NP sizes at the fixed shape.

Concluding this section let us briefly discuss the scattering of incline-incident light plane waves. Figure 14 demonstrates the scattering cross sections calculated for the 70° incidence of light waves with TM and TE polarization. In the case of the TM-polarization light [Fig. 14(a)] the partial scattering cross section $\sigma_{\rm SPP}$ exceeds the section $\sigma_{\rm Light}$ because of the contribution of the large out-of-plane ED component p_z excited by the electric field of the incident light wave. Partially the situation recalls the SPP scattering [Fig. 2(a)] where the out-of-plane ED component p_z plays a principal role. In the case of the TE-polarization light [Fig. 14(b)] the efficiency of scattering into light exceeds the scattering into SPPs as it is realized in the case of the normal-incident light. An additional resonant peak at $\lambda = 710$ nm in Fig. 14(b) corresponds to resonant excitation of the out-of-plane MD component m_z. However, as already has been indicated above, this component does not participate in the SPP excitation and can increase the only light-into-light scattering cross section.

IV. CONCLUSION

The multipole analysis of SPP and light scattering by arbitrarily shaped NPs located on a plane surface has been applied to study the optical response of individual spheroidal

silicon NPs with sizes of the order of 200 nm being placed near a gold surface. Using numerical calculations by the DDA method together with the multipole decomposition procedure, we showed that the extinction and scattering cross sections of the silicon NPs have two resonances (in the spectral range of $\lambda \in [575–825]$ nm) corresponding to the resonant excitations of their ED and MD moments. Due to the bianisotropy effect, the in-plane ED and MD components are excited by both electric and magnetic fields of incident electromagnetic waves. As a result, the resonant peaks of the extinction cross sections can include both ED and MD resonant contributions. It was found that, in the case of SPP scattering by oblate spheroidal silicon NPs, the ED and MD resonant excitations can ensure resonant unidirectional and elastic SPP scattering within the spectral range that is determined by the NP aspect ratio. For NPs with the aspect ratio of 1.8, it was obtained that at the wavelength $\lambda = 610$ nm the SPP forward (elastic) scattering is ten (five) times more effective than the SPP backward (SPP into light) scattering. The suppression of SPP scattering into light is connected with the destructive interference between light waves radiated by the induced ED and MD moments of NP.

We have also discussed a role of the bianisotropy effect in the realization of the efficient elastic SPP scattering. It was shown that due to the bianisotropy effect the contributions of the in-plane ED and MD components to the extinction cross section can be of opposite signs. In this case, the destructive interference between the waves generated by these dipole components can suppress the considered scattering channel. In the case of SPP incidence, this destructive interference practically eliminates (out-of-plane) scattering into light, whereas in the case of normally incident light this ensures efficient suppression of SPP excitation in the system. The appropriate analytical condition for the suppression of the SPP excitation has been obtained. Difference in SPP and light scattering by NPs is connected with different spatial distributions of the electric and magnetic fields created in these two cases near a gold surface. In the case of normally incident light waves, the induced ED **p** exceeds the induced MD $\sqrt{\mu_0\varepsilon_0}\,\mathbf{m}$ (where $\sqrt{\mu_0\varepsilon_0}$ is the dimension factor) within the considered spectral range [Fig. 15(a)]. As a result, only the SPP scattering suppression can be realized in the system at the short-wavelength resonance [Fig. 15(a)]. In the case of SPP scattering, the corresponding magnitudes of **p** and $\sqrt{\mu_0\varepsilon_0}\,\mathbf{m}$ can be equal to each other at the short-wavelength resonance [Fig. 15(b)], providing the possibility of suppression of SPP-into-light scattering (Fig. 8). Additionally, it was shown that, in the case of oblique light incidence, the scattering cross sections for scattering into light and SPP excitation are strongly dependent on the light polarization.

Summarizing, the results obtained demonstrate directly that high refractive index dielectric NPs (for example, crystalline silicon NPs), supporting resonant excitation of the MD and ED modes and being located on metal (gold and silver) substrates, can be used for the realization of unidirectional and elastic SPP scattering as well as for the suppression of SPP scattering when illuminated by light. We believe that these unique optical properties are very important for designing SPP-based photonic components and metasurfaces for control and manipulation of SPP and light waves.

ACKNOWLEDGMENTS

We acknowledge financial support for this work from the University of Southern Denmark (SDU 2020 funding) and from the European Research Council, Grant No. 341054 (PLAQNAP).

[1] A. V. Zayats, I. I. Smolyaninov, and A. A. Maradudin, Nano-optics of surface plasmon polaritons, Phys. Rep. **408**, 131 (2005).

[2] S. A. Maier, *Plasmonics: Fundamentals and Application* (Springer, Berlin, 2007).

[3] M. I. Stockman, Nanoplasmonics: past, present, and glimpse into future, Opt. Express **19**, 22029 (2011).

[4] S. I. Bozhevolnyi and F. A. Pudonin, Two-Dimensional Micro-Optics of Surface Plasmons, Phys. Rev. Lett. **78**, 2823 (1997).

[5] H. Ditlbacher, J. R. Krenn, G. Schider, A. Leitner, and F. R. Aussenegg, Two-dimensional optics with surface plasmon polaritons, Appl. Phys. Lett. **81**, 1762 (2002).

[6] J. R. Krenn, H. Ditlbacher, G. Schider, A. Hohenau, A. Leitner, and F. R. Aussenegg, Surface plasmon microand nano-optics, J. Microsc. **209**, 167 (2003).

[7] A. L. Stepanov, J. R. Krenn, H. Ditlbacher, A. Hohenau, A. Drezet, B. Steinberger, A. Leitner, and F. R. Aussenegg, Quantitative analysis of surface plasmon interaction with silver nanoparticles, Opt. Lett. **30**, 1524 (2005).

[8] A. B. Evlyukhin, S. I. Bozhevolnyi, A. L. Stepanov, R. Kiyan, C. Reinhardt, S. Passinger, and B. N. Chichkov, Focusing and directing of surface plasmon polaritons by curved chains of nanoparticles, Opt. Express **15**, 16667 (2007).

[9] I. P. Radko, S. I. Bozhevolnyi, A. B. Evlyukhin, and A. Boltasseva, Surface plasmon polariton beam focusing with parabolic nanoparticle chains, Opt. Express **15**, 6576 (2007).

[10] I. P. Radko, V. S. Volkov, J. Beermann, A. B. Evlyukhin, T. Søndergaard, A. Boltasseva, and S. I. Bozhevolnyi, Plasmonic metasurfaces for waveguiding and field enhancement, Laser Photon. Rev. **3**, 575 (2009).

[11] T. Søndergaard and S. I. Bozhevolnyi, Surface plasmon polariton scattering by a small particle placed near a metal surface: An analytical study, Phys. Rev. B **69**, 045422 (2004).

[12] A. B. Evlyukhin and S. I. Bozhevolnyi, Point-dipole approximation for surface plasmon polariton scattering: Implications and limitations, Phys. Rev. B **71**, 134304 (2005).

[13] T. Søndergaard and S. I. Bozhevolnyi, Vectorial model for multiple scattering by surface nanoparticles via surface polariton-to-polariton interactions, Phys. Rev. B **67**, 165405 (2003).

[14] A. I. Kuznetsov, A. B. Evlyukhin, C. Reinhardt, A. Seidel, R. Kiyan, W. Cheng, A. Ovsianikov, and Boris N. Chichkov, Laser-induced transfer of metallic nanodroplets for plasmonics and metamaterial applications, J. Opt. Soc. Am. B **26**, B130 (2009).

[15] A. V. Shchegrov, I. V. Novikov, and A. A. Maradudin, Scattering of Surface Plasmon Polaritons by a Circularly Symmetric Surface Defect, Phys. Rev. Lett. **78**, 4269 (1997).

[16] C. F. Bohren and D. R. Huffman, *Absorption and Scattering of Light by Small Particles* (Wiley, New York, 2008).
[17] A. B. Evlyukhin, C. Reinhardt, A. Seidel, B. S. Luk'yanchuk, and B. N. Chichkov, Optical response features of Si-nanoparticle arrays, Phys. Rev. B **82**, 045404 (2010).
[18] A. Garcia-Etxarri, R. Gomez-Medina, L. S. Froufe-Perez, C. Lopez, L. Chantada, F. Scheffold, J. Aizpurua, M. Nieto-Vesperinas, and J. J. Saenz, Strong magnetic response of submicron silicon particles in the infrared, Opt. Express **19**, 4815 (2011).
[19] A. B. Evlyukhin, S. M. Novikov, U. Zywietz, R. L. Eriksen, C. Reinhardt, S. I. Bozhevolnyi, and B. N. Chichkov, Demonstration of magnetic dipole resonances of dielectric nanospheres in the visible region, Nano Lett. **12**, 3749 (2012).
[20] A. I. Kuznetsov, A. E. Miroshnichenko, Y. H. Fu, J. Zhang, and B. Luk'yanchuk, Magnetic light, Sci. Rep. **2**, 492 (2012).
[21] M. Kerker, D.-S. Wang, and C. Giles, Electromagnetic scattering by magnetic spheres, J. Opt. Soc. Am. **73**, 765 (1983).
[22] Y. H. Fu, A. I. Kuznetsov, A. E. Miroshnichenko, Y. F. Yu, and B. Luk'yanchuk, Directional visible light scattering by silicon nanoparticles, Nature Commun. **4**, 1527 (2013).
[23] A. B. Evlyukhin, C. Reinhardt, and B. N. Chichkov, Multipole light scattering by nonspherical nanoparticles in the discrete dipole approximation, Phys. Rev. B **84**, 235429 (2011).
[24] I. Staude, A. E. Miroshnichenko, M. Decker, N. T. Fofang, S. Liu, E. Gonzales, J. Dominuez, T. S. Luk, D. N. Neshev, I. Brener, and Y. S. Kivshar, Tailoring directional scattering through magnetic and electric resonances in subwavelength silicon nanodisks, ACS Nano **7**, 7824 (2013).
[25] Y. F. Yu, A. Y. Zhu, R. Paniagua-Domínguez, Y. H. Fu, B. Luk'yanchuk, and A. I. Kuznetsov, High-transmission dielectric metasurface with 2π phase control at visible wavelengths, Laser Phot. Rev. **9**, 412 (2015).
[26] M. Decker, I. Staude, M. Falkner, J. Dominguez, D. N. Neshev, I. Brener, T. Pertsch, and Y. S. Kivshar, High-efficiency dielectric Huygens' surfaces, Adv. Opt. Mater. **3**, 813 (2015).
[27] A. E. Krasnok, A. E. Miroshnichenko, P. A. Belov, and Y. S. Kivshar, All-dielectric optical nanoantennas, Opt. Express **20**, 20599 (2012).
[28] B. Rolly, B. Stout, and N. Bonod, Boosting the directivity of optical antennas with magnetic and electric dipolar resonant particles, Opt. Express **20**, 20376 (2012).
[29] M. K. Schmidt, R. Esteban, J. J. Saenz, I. Suarez-Lacalle, S. Mackowski, and J. Aizpurua, Dielectric antennas—a suitable platform for controlling magnetic dipolar emission, Opt. Express **20**, 13636 (2012).
[30] P. Spinelli, M. A. Verschuuren, and A. Polman, Broadband omnidirectional antireflection coating based on subwavelength surface Mie resonators, Nature Commun. **3**, 692 (2012).
[31] M. L. Brongersma, Y. Cui, and S. Fan, Light management for photovoltaics using high-index nanostructures, Nat. Mater. **13**, 451 (2014).
[32] A. B. Evlyukhin, G. Brucoli, L. Martín-Moreno, S. I. Bozhevolnyi, and F. J. García-Vidal, Surface plasmon polariton scattering by finite-size nanoparticles, Phys. Rev. B **76**, 075426 (2007).
[33] A. B. Evlyukhin, C. Reinhardt, E. Evlyukhin, and B. N. Chichkov, Multipole analysis of the light scattering by arbitrary-shaped nanoparticles on a plane surface, J. Opt. Soc. Am. B **30**, 2589 (2013).
[34] B. T. Draine, The discrete-dipole approximation and its application to interstellar graphite grains, Astrophys. J. **333**, 848 (1988).
[35] P. B. Johnson and R. W. Christy, Optical constants of the noble metals, Phys. Rev. B **6**, 4370 (1972).
[36] E. Palik, *Handbook of Optical Constant of Solids* (Academic, San Diego, 1985).
[37] A. E. Miroshnichenko, A. B. Evlyukhin, Y. S. Kivshar, and B. N. Chichkov, Substrate-induced resonant magnetoelectric effects for dielectric nanoparticles, ACS Photonics **2**, 1423 (2015).
[38] E. Xifré-Pérez, L. Shi, U. Tuzer, R. Fenollosa, F. Ramiro-Manzano, R. Quidant, and F. Meseguer, Mirror-image-induced magnetic modes, ACS Nano **7**, 664 (2013).